Complete Momentum-Balance Analysis of Permeate Flux for Ultrafiltration in Hollow-Fiber Modules

Tung-Wen Cheng* and Ho-Ming Yeh

Department of Chemical and Materials Engineering, Tamkang University, Tamsui, Taiwan 251, R.O.C.

Abstract

The predicting equations for the declines of transmembrane pressure and permeate flux in hollow-fiber ultrafilters were derived from the complete momentum balance with the consideration of the rate of momentum transfer by convection, instead of simply applying Hagen-Poiseuille theory without the consideration of the effect of permeation on fluid flow, resulting in improved prediction. The assumption of laminar flow in the fiber tubes was examined.

***Key Words*:** Ultrafiltration, Hollow Fiber, Momentum Balance, Permeate Flux

1. Introduction

Recently, membrane ultrafiltration is applied in a wide variety of fields, from the chemical industry (such as electrocoat paint recovery, latex processing, textile size recovery and recovery of lubricating oil) to medical applications (such as kidney dialysis operations), and even to biotechnology applications (such as concentration of milk, egg white, juice, pectin and sugar, and recovery of protein form cheese whey, animal blood, gelatin and glue) [1,2].

Industrial uses of membrane technology have a choice of four basic designs of equipment: (i) tubular, (ii) hollow fiber, (iii) plate-type units and (iv) spiral-wound modules. In the hollow-fiber modules, membrane is formed on the inside of tiny polymer cylinders that are then bundled and potted into a tube-and-shell arrangement. The advantages of this arrangement are low cost of investment and operation, easy flow control and cleaning, and high specific surface area per unit volume.

Ultrafiltration is primarily a size-exclusion-based pressure-driven membrane separation process, the pressure applied to the working fluid provides the driving potential to force the solvent to flow through the membrane. During operation, solutes that are rejected by the membrane accumulate on the membrane surface and form a concentration polarization layer there. At steady state, the quantity of solutes conveyed by the solvent to the membrane is equal to those that diffuse back. A number of mathematic models are available in the literature that attempt to describe the mechanism of transport through membranes. Permeate flux is conventionally analyzed by use of following models: the gel-polarization model [3–9], the osmotic-pressure model [10–18], and the resistance-in-series model [19–26].

In the gel polarization model, permeate flux is reduced by the hydraulic resistance of the gel layer, and this model applies only to the system with very high concentration of solute accumulated on the membrane surface. In the osmotic pressure model, permeate flux reduction results from the decrease in effective transmembrane pressure that occurs as the osmotic pressure of the retentate increases. Accordingly, the analysis is rather difficult because the variation of concentrations at both sides of the membrane surface should be known a priori. In the resistance-in-series model, permeate flux decreases due to the resistances caused by fouling or solute adsorption and concentration polarization/gel layer. This model easily describes the relationship of permeate flux with the operating parameters, as described in Section

*Corresponding author. E-mail: twcheng@mail.tku.edu.tw

2.4. In present study, therefore, the permeate flux in hollow-fiber modules was analyzed by the resistance-in-series model coupled with the use of complete momentum balance.

2. Theory

Consider a hollow-fiber module with N fibers of same size, in which the membrane is formed on the inside of N tiny porous tubes that are then bundled and potted into a tube-and-shell arrangement, as shown in Figure 1, while Figure 2 shows the flows and fluxes in the fiber tube of radius r_m and length L.

2.1 Mass Balance

Let $q(z)/N$ be the volumetric rate of solution in a hollow-fiber and $J(z)$ be the permeate flux by ultrafiltration. Then a mass balance over slice dz of the fiber gives

$$\frac{d(q/N)}{dz} = -2\pi r_m J(z) \tag{1}$$

2.2 Momentum Balance

For the steady-state operation, the momentum balance within the differential length dz of a hollow fiber is [27]

$$\frac{d}{dz}(\rho u_b^2) + \frac{d}{dz}(\Delta p) + \frac{\tau_s(2\pi r_m)}{\pi r_m^2} = 0 \tag{2}$$

where Δp $(= p - p_s)$ denotes the transmembrane pressure, and $p(z)$ and p_s are the pressures in fiber tubes and shell sides, respectively, while the shear stress τ_s relates to the friction factor f and bulk velocity u_b as

$$\tau_s = (\rho u_b^2/2) f \tag{3}$$

For laminar flow,

$$f = 16/(2r_m u_b \rho/\mu) \tag{4}$$

and for flow in a fiber tube

$$q/N = \pi r_m^2 u_b \tag{5}$$

Finally, Eq. (2) can be rewritten as

$$\frac{\rho}{\pi^2 r_m^4}\frac{d(q/N)^2}{dz} + \frac{d(\Delta p)}{dz} + \frac{8\mu(q/N)}{\pi r_m^4} = 0 \tag{6}$$

In the previous works [21–25], the momentum balance was taken inaccurately by neglecting the rate of momentum by convection, the first term in Eq. (6).

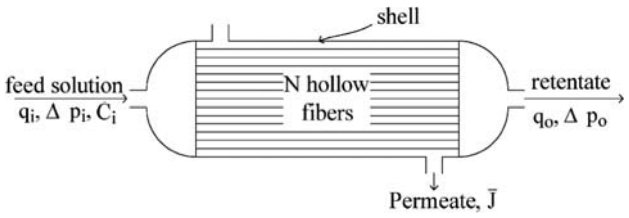

Figure 1. Hollow fiber ultrafilter.

2.3 Pressure Declination

For mathematical simplicity, we define the following dimensionless groups:

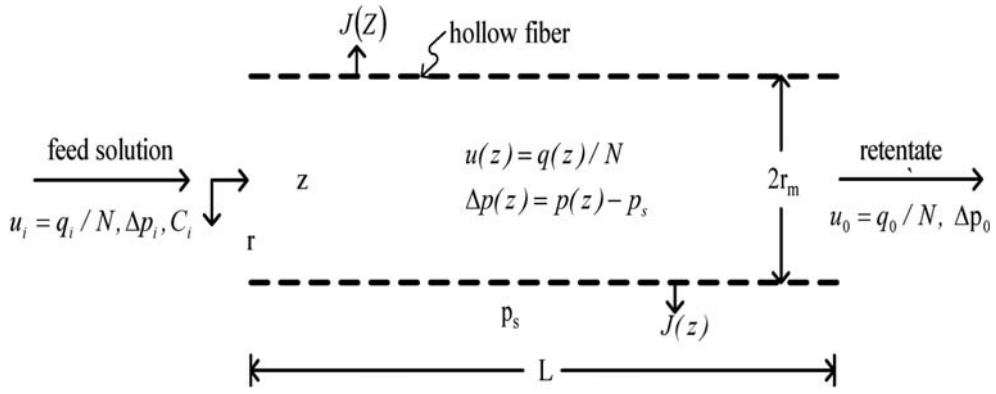

Figure 2. Flow and fluxes in a hollow fiber for ultrafiltration.

$$Q = \frac{8\mu L(q/N)}{\pi r_m^4(\Delta p_i)} \tag{7}$$

$$\Delta P = \frac{\Delta p}{\Delta p_i} \tag{8}$$

$$Z = \frac{z}{L} \tag{9}$$

Since for ultrafiltration, the amount of permeate is extremely less then the flow rate, i.e.

$$q/N >> \int_0^L 2\pi r_m J(z)dz = 2\pi r_m L\overline{J} \tag{10}$$

Thus, $J(z)$ in Eq. (1) may be taken approximately as its average value, i.e.

$$\overline{J} = \frac{1}{L}\int_0^L J(z)dz \tag{11}$$

and Eqs. (1) and (6) become, with the use of Eqs. (7)–(9)

$$\frac{dQ}{dZ} = -\alpha \tag{12}$$

$$\gamma\frac{dQ^2}{dZ} + \frac{d\Delta P}{dZ} + Q = 0 \tag{13}$$

where

$$\alpha = \frac{16\mu L^2\overline{J}}{r_m^3(\Delta p_i)} \tag{14}$$

$$\gamma = \frac{\rho r_m^4(\Delta p_i)}{64\mu^2 L^2} \tag{15}$$

Integrating Eq. (12) with the inlet conditions:

$$Q = Q_i(q = q_i) \text{ at } Z = 0 \tag{16}$$

One has

$$Q = Q_i - \alpha Z \tag{17}$$

Substituting Eq. (17) into Eq. (13) and integrating with inlet condition:

$$\Delta P = 1\ (\Delta p = \Delta p_i) \text{ at } Z = 0 \tag{18}$$

this gives

$$\Delta P = 1 + (2\alpha\gamma - 1)Q_i Z + (\alpha/2 - \alpha^2\gamma)Z^2 \tag{19}$$

2.4 Permeate Flux

Since membrane ultrafiltration is a pressure-driven separation, the pressure applied to the working fluid provides the driving potential to force the permeate to flow through the membrane. Therefore,

$$J = 0, \text{ for } \Delta p = 0 \tag{20}$$

For a small applied pressure, the permeate flux through the membrane is observed to be proportional to the applied pressure, i.e.

$$J = (\text{constant})\Delta p, \text{ for small } \Delta p \tag{21}$$

However, as the pressure is increased, the flux begins to drop below a linear flux-pressure behavior. Eventually, a limiting flux, J_{lim}, is reached where any further pressure increase no longer results in any increase in flux, i.e.

$$J = J_{lim}, \text{ as } \Delta p \to \infty \text{ (or large enough)} \tag{22}$$

According to above description, the following resistance-in-series for permeate flux may be introduced:

$$J = \frac{\Delta p}{R_m + R_f + \Delta p/J_{\lim}} \tag{23}$$

where R_m denotes the intrinsic resistance of membrane, R_f is the resistance due to fouling phenomena, while $\Delta p/J_{lim}$ is the resistance due to the concentration polarization, which will be proportional to the compressible layer deposited and may be assumed to be a linear function of transmembrane pressure with ϕ (= $1/J_{lim}$) as a proportional constant.

Eq. (23) may be rewritten as

$$V = 1 - \frac{1}{1+\beta\Delta P} \tag{24}$$

where

$$V = J/J_{lim} \tag{25}$$

$$\beta = (\Delta p_i)/[(R_m + R_f)\, J_{lim}] \tag{26}$$

and the average permeate flux, Eq. (11), may be rewritten as

$$\overline{V} = \int_0^1 V dZ \tag{27}$$

Substitution of Eqs. (19) and (24) into Eq. (27) gives

$$\overline{V} = 1 - \int_0^1 \frac{dZ}{AZ^2 + BZ + C} \tag{28}$$

$$= 1 - \frac{2}{\sqrt{4AC - B}} \left[\tan^{-1}\left(\frac{2A + B}{\sqrt{4AC - B^2}} \right) - \tan^{-1}\left(\frac{B}{\sqrt{4AC - B^2}} \right) \right], \quad B^2 < 4AC \tag{29}$$

$$= 1 - \frac{1}{\sqrt{B^2 - 4AC}} \ln \left| \frac{\left(2A + B - \sqrt{B^2 - 4AC}\right)\left(B + \sqrt{B^2 - 4AC}\right)}{\left(2A + B + \sqrt{B^2 - 4AC}\right)\left(B - \sqrt{B^2 - 4AC}\right)} \right|, \quad B^2 > 4AC \tag{30}$$

where

$$A = \beta \left(\alpha/2 - \alpha^2 \gamma \right) \tag{31}$$

$$B = \beta\, (2\alpha\gamma - 1) Q_i \tag{32}$$

$$C = 1 + \beta \tag{33}$$

3. Determination of J_{lim} and R_j

It was found that according to Eq. (23) and with the experimental data at certain flow velocity u_i and feed concentration C_i, a straight line of $\left(1/\overline{J}_{exp}\right)$ versus $1/(\overline{\Delta p})_{exp}$ could be constructed, as described by Eq. (34), with the use of the least-squares method [21,22]. Therefore, the experimental values of $(R_m + R_f)$ and $1/J_{lim}$ can be obtained, respectively, as slope and the intersection at the ordinate, where $(\overline{\Delta p})_{exp} = \infty$. After obtaining the experimental values of $(R_m + R_f)$ and $1/J_{lim}$ at various feed concentrations, C_i, and velocities, u_i. The correlation equations of relating $(R_m + R_f)$ and $1/J_{lim}$ with the operating parameters C_i and u_i can be determined by the least-squares method [21,22].

$$\frac{1}{\overline{J}_{\exp}} = \frac{1}{J_{\lim}} + (R_m + R_f)/(\Delta p)_{\exp} \tag{34}$$

4. Comparison of Correlation Prediction for Permeate Flux

A comparison of permeate flux may be made by using the experimental data of Dong's work [28], Table 1, for ultrafiltration of dextran T500 aqueous solution in an Amicon model H1P30-20 hollow-fiber cartridge (Amicon Corp., Danvers, MS). From the dimensions of module used, $r_m = 2.5 \times 10^{-4}$ m, L = 0.153 m, and N = 250. In addition, the viscosity of dextran T500 aqueous solution at 25 °C may be estimated by [29],

$$\mu = 0.894 \times 10^{-3} e^{0.408 C_i} \ (\text{Pa} \cdot \text{s}) \text{ or } (\text{kg/m} \cdot \text{s}) \tag{35}$$

and the correlation equation for $(R_m + R_f)$ and J_{lim} were determined by the method described in the pervious section with the use of experimental data as

$$R_m + R_f = 3.67\,(1 + 0.45\, u_i^{-0.025}\, C_i^{0.23}) \times 10^9 \ (\text{Pa} \cdot \text{s/m}) \tag{36}$$

$$J_{lim} = 3.66 \times 10^{-6}\, C_i^{-0.375} \ (\text{s/m}) \tag{37}$$

in which

$$u_i = \frac{q_i}{N\pi r_m^2} = 2.037 \times 10^4 q_i \ (\text{m/s}) \tag{38}$$

Some correlation predictions for average permeate flux were calculated and the results are compared with the experimental results, as shown in Figures 3–5. It is seen from these figures that the predicting values are in fairly good agreement with the experimental results of present interest.

5. Discussion and Conclusion

The predicting equations, Eqs. (29) and (30), for the

Table1. Experimental data for average permeate flux $\bar{J}$ (m^3/m^2s) [28]

q_i ($\times 10^6\ m^3/s$)	Δp_i ($\times 10^{-5}\ Pa$)	$C_i = 0$		$C_i = 0.1wt\ \%$		$C_i = 0.2wt\ \%$		$C_i = 0.5wt\ \%$		$C_i = 1.0wt\ \%$	
		Δp_0 (Pa)	$\bar{J} \times 10^6$	Δp_0 (Pa)	$\bar{J} \times 10^6$	Δp_0 (Pa)	$\bar{J} \times 10^6$	Δp_0 (Pa)	$\bar{J} \times 10^6$	Δp_0 (Pa)	$\bar{J} \times 10^6$
5.0	0.3	0.194	6.822	0.190	2.115	0.190	2.218	0.186	1.862	0.190	1.673
	0.5	0.388	12.318	0.380	3.682	0.384	3.536	0.376	2.811	0.380	2.252
	0.7	0.582	18.116	0.574	4.861	0.574	4.246	0.570	3.366	0.572	2.590
	1.0	0.874	23.020	0.862	5.767	0.862	4.755	0.858	3.680	0.854	2.738
	1.2	0.964	28.539	1.052	6.114	1.056	4.978	1.048	3.740	1.046	2.782
	1.4	1.252	35.997	1.246	6.391	1.246	5.182	1.242	3.842	1.238	2.825
	1.6			1.436	6.577	1.438	5.371	1.434	3.955	1.430	2.849
7.5	0.3			0.176	2.067	0.178	2.188	0.176	1.863	0.170	1.704
	0.5			0.372	3.623	0.372	3.684	0.366	3.111	0.360	2.487
	0.7			0.562	4.919	0.562	4.643	0.558	3.767	0.552	2.864
	1.0			0.848	6.175	0.850	5.330	0.846	4.245	0.838	3.148
	1.2			1.040	6.745	1.044	5.456	1.040	4.406	0.972	3.206
	1.4			1.232	7.012	1.238	5.604	1.230	4.505	1.028	3.277
	1.6			1.428	7.282	1.428	5.789	1.422	4.548	1.220	3.381
10.0	0.3			0.166	2.229	0.160	2.036	0.156	2.421	0.148	1.767
	0.5			0.356	4.044	0.402	3.721	0.348	3.201	0.338	2.788
	0.7			0.548	5.633	0.794	4.816	0.538	3.969	0.524	3.345
	1.0			0.840	7.041	0.882	5.702	0.828	4.546	0.812	3.683
	1.2			1.030	7.617	1.074	6.026	1.022	4.747	1.004	3.831
	1.4			1.222	8.024	1.266	6.228	1.214	4.791	1.196	3.887
	1.6			1.414	8.284	1.458	6.388	1.404	4.856	1.388	3.993

average permeate fluxes of membrane ultrafiltration in hollow fiber modules was derived from mass and momentum balances based on the resistance-in-series model with the consideration of momentum fluxes due to convection (fluid motion). The declines of transmembrane pressure and permeate flux along the flow channel can be predicted from Eqs. (19) and (24), respectively. Some predicted values for the average permeate fluxes are presented in Figures 3–5, comparing with the experimental results. It is seen in these figures that the predicted results are in good agreement with the experimental results at high transmembrane-pressure operation, but are overestimated at low transmembrane-pressure operation. This may be because that the assumption of a linear function of transmembrane pressure for the concentration polarization resistance is not suitable for the ultrafiltration at the lower transmembrane-pressure operation. The modification of this term in the resistance-in-series model will be our next research work.

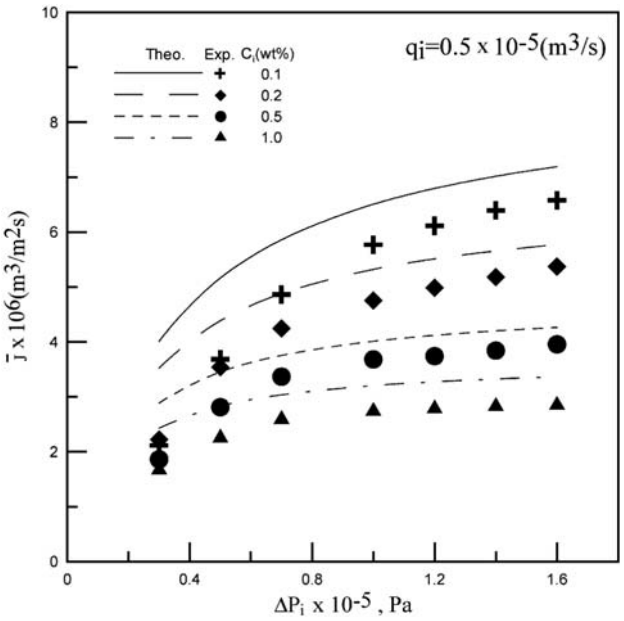

Figure 3. Average permeate fluxes for $q_i = 0.5 \times 10^{-5}$ m^3/s.

In the previous studies, the momentum balance was taken inaccurately by simply applying Hagen-Poiseuille theory without the consideration of the effect of permeate flux loss on momentum balance, as well as neglecting the loss of momentum flux due to convection. In present study, however, we analyzed the declines of

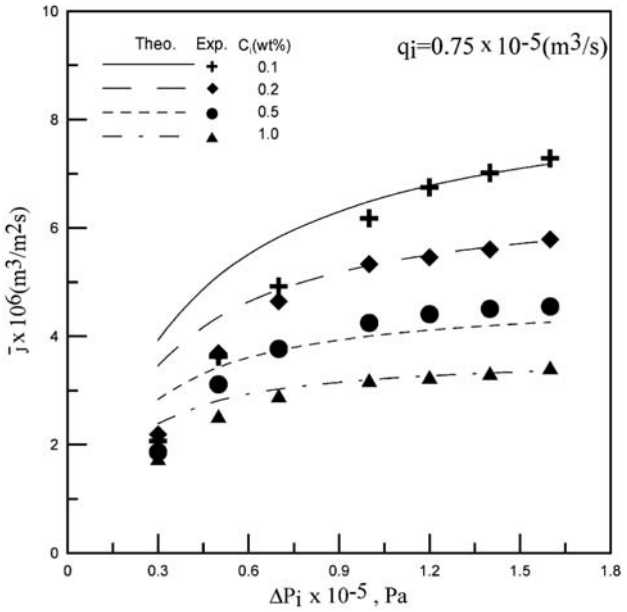

Figure 4. Average permeate fluxes for $q_i = 0.75 \times 10^{-5}$ m^3/s.

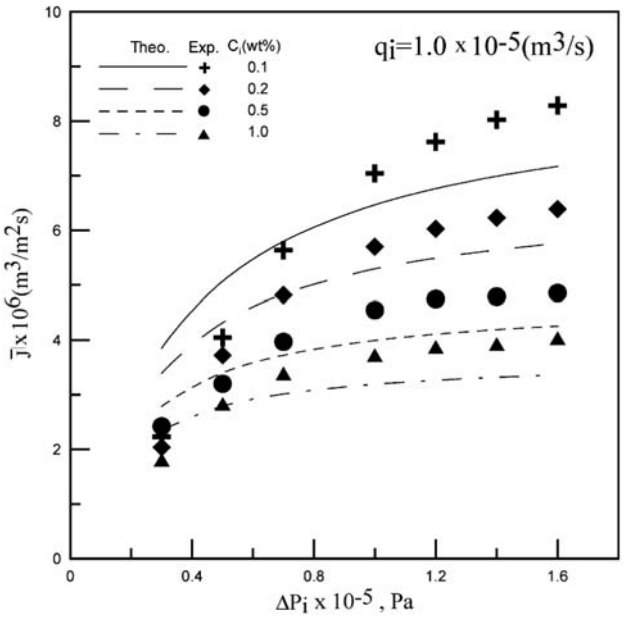

Figure 5. Average permeate fluxes for $q_i = 1.0 \times 10^{-5}$ m^3/s.

transmembrane pressures and permeate flux with the consideration of the loss of momentum flux due to fluid motion, as indicated by the first term in Eq. (6). The correlation predictions thus obtained will be more accurate for the high permeate-flux operations. Further, the resistance-in series model satisfies the three essential conditions of membrane ultrafiltration, Eqs. (20)–(22). Therefore, the present modeling study easily describes the relationships of permeate flux with operating and design parameters, and we believe that it will also be suitable for most membrane ultrafiltration systems including systems with different kinds of feed solutions, different materials of membrane tubes and various design and operating conditions.

Finally, the assumption of laminar flow should be checked with the maximum value of Reynolds number. The critical case may be that of $C_i = 0.1$ *wt* % and $q_i = 1 \times 10^{-5}$ m^3/s with $r_m = 2.5 \times 10^{-4}$ m, $N = 250$, $\rho = 1 \times 10^3$ kg/m^3, and $\mu = 0.894 \times 10^{-3} \exp(0.408C_i)$ (Pa · s or kg/m · s) Pa [29], The result is

$$(R_e)_{\max} = \frac{2r_m(q_i / N\pi r_m^2)\rho}{\mu} = 98 < 2100$$

Therefore, the assumption of laminar flow is acceptable for the system of present interest.

Nomenclature

C_i	concentration of feed solution (wt% dextran T500)
J	permeate flux of solution (m^3/m^2s)
J_{lim}	limiting flux (m^3/m^2s)
L	effective length of hollow fiber (m)
N	number of hollow fibers in a membrane module
p	pressure distribution on the tube side (Pa)
p_s	uniform permeate pressure on the shell side (Pa)
Δp	transmembrane pressure, $p-p_s$ (Pa)
ΔP	dimensionless transmembrane pressure, $\Delta p/\Delta p_i$
Q	dimensionless flow rate, defined by Eq. (12)
q	volume flow rate in a hollow-fiber module (m^3/s)
R_f	resistance due to solute adsorption and fouling (Pa.s/m)
R_m	intrinsic resistance of membrane (Pa.s/m)
r_m	inside radius of hollow fiber (m)
u	fluid velocity in the hollow fiber, $q / N(\pi r_m^2)$ (m/s)
V	dimensionless permeate flux, defined by Eq. (25)
ν_m	permeate flux of solution ($m^3/m^2.s$)
$\nu_{m,lim}$	limiting flux ($m^3/m^2.s$)
Z	dimensionless axial coordinate, z/L
z	axial coordinate (m)

Greek letters

α	dimensionless group, defined by Eq. (14)
β	dimensionless group, defined by Eq. (26)

γ dimensionless group, defined by Eq. (15)
μ viscosity of solution (Pa.s)
ϕ a proportional constant, $1/J_{lim}$, defined in Eq. (23) (m^2s/m^3)

Subscripts

b bulk
i at the inlet
o at the outlet

Superscript

– average value

References

[1] Poter M. C., *Membrane Filtration, Handbook of Separation Techniques for Chemical Engineers,* Schweitzer, P. A., ed., McGraw-Hill New York, Sec. 2.1 (1979).

[2] Cheryan, M., *Ultrafiltration Handbook,* Technomic Publishing, Lancaster, Pennsylvania, Sec. 8. (1986)

[3] Blatt, W. F., Dravid, A., Michales, A. S. and Nelsen L., "Solute Polarization and Cake Formation in Membrane Ultrafiltration: Causes, Consequences and Control Technique," *Membrane Science and Technology,* Filnn, J. E., ed., Plenum Press, New York, p. 47 (1970).

[4] Poter, M. C., "Concentration Polarization with Membrane Ultrafiltration," *Ind. Eng. Chem. Proc. Res. Dev.,* Vol. 11, p. 234 (1972).

[5] Grieves, R. B., Bhattacharyya, D., Schomp, W. G. and Bewley, J. L., "Membrane Ultrafiltration of Nonionic Surfactant," *AIChE J.,* Vol. 19, p. 766 (1973).

[6] Shen, J. J. S. and Probstein, R. F., "On the Prediction of Limiting Flux in Laminar Ultrafiltration of Macromolecular Solution," *Ind. Eng. Chem. Fundam.,* Vol. 16, p. 459 (1977).

[7] Nokao, S., Nomura, T. and Kimura, S., "Characteristics of Macromolecular Gel Layer Formed on Ultrafiltration Tubular Membrane," *AIChE J.,* Vol. 25, p. 615 (1979).

[8] Fane, A. G., Fell, C. J. D. and Waters, A. G., "The Relationship between Membrane Surface Pore Characteristics and Flux Ultrafiltration Membranes," *J. Membr. Sci.,* Vol. 9, p. 245 (1981).

[9] Fane, A. G., "Ultrafiltration of Suspensions," *J. Membr. Sci.,* Vol. 20, p. 249 (1984).

[10] Wijmans, J. G., Nakao, S. and Smolders C. A., "Flux Limitation in Ultrafiltration: Osmotic Pressure Model and Gel Layer Model," *J. Membr. Sci.,* Vol. 20, p. 115 (1984).

[11] Kozinski, A. A. and Lighfoot, E. N., "Protein Ultrafiltration: A General Example of Boundary Layer Filtration," *AIChE J.,* Vol. 19, p. 1030 (1972).

[12] Leung, W., and Probstein, R. F., "Low Polarization in Laminar Ultrafiltration of Macromolecular Solutions," *Ind. Eng. Chem. Fundam.,* Vol. 18, p. 274 (1979).

[13] Wendt, R. P., Klein, E., Holland, F. F. and Eberle, K. E., "Hollow Fiber Ultrafiltration of Calf Serum and Albumin in the Pregel Uniform-Wall-Flux Region," *Chem. Eng. Commun.,* Vol. 8, p. 251 (1981).

[14] Nakao, S. and Kimura, S., "Models of Membrane Transport Phenomena and their Applications for Ultrafiltration Data," *J. Chem. Eng. Jpn.,* Vol. 15, p. 200 (1982).

[15] Kleinstreuer, C. and Paller, M. S., "Laminar Dilute Suspension Flows in Plate-and-Frame Ultrafiltration Units," *AIChE J.,* Vol. 29, p. 529 (1983).

[16] Clifton, M. J., Abidine, N., Aptel, P. and Sanchez, V., "Growth of the Polarization Layer in Ultrafiltration with Hollow-Fiber Membranes," *J. Membr. Sci.,* Vol. 21, p. 233 (1984).

[17] Ma, R. P., Gooding, C. H. and Alexander, W. K., "A Dynamic Model for Low-Pressure, Hollow Fiber Ultrafiltration," *AIChE J.,* Vol. 31, p. 1728 (1985).

[18] Nabetani, H., Nakajima, M., Watanabe, A., Nakao, S. and Kumura, S., "Effects of Osmotic Pressure and Adsorption on Ultrafiltration of Ovalbumin," *AIChE J.,* Vol. 36, p. 907 (1990).

[19] Chiang, B. H. and Cheryan, M., "Ultrafiltration on Skin Milk in Hollow Fibers," *J. Food Sci.,* Vol. 51, p. 340 (1986).

[20] Assadi, M. and White, D. A., "A Mode for Determining the Steady-State Flux of Inorganic Microfiltration Membrane," *Chem. Eng. J.,* Vol. 48, p. 11 (1992).

[21] Yeh, H. M. and Cheng, T. W., "Resistance-in-Series of Membrane Ultrafiltration in Hollow Fiber of Tube-and-Shell Arrangement," *Sep. Sci. Technol.,* Vol. 28, p. 1341 (1993).

[22] Yeh, H. M. and Wu, H. H., "Membrane Ultrafiltration in Combined Hollow-Fiber Module Systems," *J.*

Membr. Sci., Vol. 124, p. 93 (1997).

[23] Yeh, H. M. and Tsai, J. W., "Membrane Ultrafiltration in Multipass Hollow-Fiber Modules," *J. Membr. Sci.*, Vol. 142, p. 61 (1998).

[24] Yeh, H. M., Chen, H. Y. and Chen, K. T., "Membrane Ultrafiltration in Tubular Module with a Steel Rod Inserted Concentrically for Improved Performance," *J. Membr. Sci.,* Vol. 168, p. 121 (2000).

[25] Yeh, H. M. and Chen, K. T., "Improvement of Ultrafiltration Performance in Tubular Membranes using a Twisted Wired-Rod Assembly," *J. Membr. Sci.,* Vol. 178, p. 43 (2000).

[26] Yeh, H. M., Dong, J. F., Hsieh, M. J. and Yang, C. C., "Prediction of Permeate Flux for Ultrafiltraction in a Wire-Rod Tubular-Membrane Modules," *J. Membr. Sci.,* Vol. 209, p. 19 (2002).

[27] Bird, R. B., Stewart, W. E. and Lightfoot, E. N., *Transport Phenomena*, Wiley, New York, p. 44 (1971).

[28] Dong, J. F., "Permeate Flux Analysis for Membrane Ultrafiltration," M. S. thesis, Tamkang University, Tamsui, Taiwan (2001).

[29] Cheng, T. W., "A Study on the Hollow-Fiber Membrane Ultrafiltration," Ph.D. thesis, National Taiwan University, Taipei, Taiwan, p. 146 (1992).

Manuscript Received: Apr. 26, 2005
Accepted: May. 20, 2006